materials

MDPI

Article

The Effect of Heat Treatment after Hydrothermal Reaction on the Lithium Storage Performance of a MoS_2/Carbon Cloth Composite

Xintong Li, Chonggui Li * and Qi Yang

School of Materials Science and Engineering, Shanghai University of Engineering Science, Shanghai 201620, China
* Correspondence: chongguili@sues.edu.cn

Abstract: In this study, 1T phase MoS_2 nanosheets were synthesized on the surface of a carbon cloth via a hydrothermal reaction. After heat treatment, the 1T phase MoS_2 was transformed into the 2H phase with a better capacity retention performance. As an anode material for lithium-ion batteries, 2H phase MoS_2 on the carbon cloth surface delivers a capacity of 1075 mAh g^{-1} at a current density of 0.1 A g^{-1} after 50 cycles; while the capacity of the 1T phase MoS_2 on the surface of the carbon cloth without heat treatment fades to 528 mAh g^{-1}. The good conductivity of a carbon cloth substrate and the separated MoS_2 nanosheets help to increase the capacity of MoS_2 and decrease its charge transfer resistance and promote the diffusion of lithium ions in the electrode.

Keywords: molybdenum disulfide; carbon cloth; heat treatment; anode material; lithium-ion batteries

Citation: Li, X.; Li, C.; Yang, Q. The Effect of Heat Treatment after Hydrothermal Reaction on the Lithium Storage Performance of a MoS_2/Carbon Cloth Composite. *Materials* **2023**, *16*, 7678. https://doi.org/10.3390/ma16247678

Academic Editor: Christof Schneider

Received: 4 November 2023
Revised: 7 December 2023
Accepted: 13 December 2023
Published: 17 December 2023

1. Introduction

Since the invention of lithium-ion batteries (LIBs) in 1991, they have become the primary power source for portable electronic devices due to their high-energy density, good cycling stability, and long service life [1,2]. In recent years, due to the development of electric vehicles, material scientists have been required to develop LIBs with higher energy density [3–5]. However, the currently commercialized graphite anode material cannot meet the increasing energy density requirements of LIBs because of its low theoretical capacity (372 mAh g^{-1}) [6]. Transition metal sulfides with a higher theoretical capacity than the graphite anode material have attracted considerable attention [7–9]. As one of transition metal sulfides, MoS_2 has a theoretical specific capacity (670 mAh g^{-1}), which is 1.8 times the theoretical capacity of graphite [10–12]. MoS_2 has a layered structure. Single-layer MoS_2 consists of two layers of sulfur atoms sandwiched by a layer of molybdenum atoms [13]. Multilayer MoS_2 is composed of several single-layer MoS_2 connections, with a spacing of ~0.65 nm between layers. The layered structure of MoS_2 facilitates the diffusion of lithium ions in the electrode and buffers the volume change during charge–discharge, which leads to its good cyclic reversibility [14,15]. However, as an inorganic material, MoS_2 has poor conductivity. Ammonium molybdate, which is commonly used as a raw material for the hydrothermal synthesis of MoS_2, is readily soluble in water but not in organic solvents. Due to the strong polarity of water, MoS_2 synthesized with the hydrothermal method is prone to agglomerate. Large-sized aggregates will decrease the sites of electrochemical reactions and increase the diffusion distance of lithium ions in the electrode, resulting in a reduction in their electrochemical performance. Therefore, determining how to improve the conductivity of MoS_2 and how to synthesize its nanostructures is an important strategy to enhance its electrochemical performance.

Carbonaceous materials have good conductivity, and their volume effect during charge–discharge is small [16,17]. Thus, as substrates, carbonaceous materials can improve the conductivity of transition metal sulfides and buffer their volume changes. A carbon

cloth is a flexible carbonaceous material woven with carbon fibers [18]. Its good conductivity and mechanical flexibility make it an appropriate collector for flexible LIB electrodes.

Recently, there are some studies on the synthesis and lithium storage performance of MoS_2/carbon cloth composites. Some effective strategies, such as the preparation of ultra-thin MoS_2 nanosheets, the fabrication of 3D graphene/MoS_2 spherical heterostructure [19], the N doping of MoS_2 [20], the preparation of CdS@MoS_2 core-shell structured nanospheres [21], and the P doping of MoS_2 [22] have been conducted to improve the lithium storage performance of MoS_2/carbon cloth composites. However, the effect of heat treatment after the hydrothermal reaction on their lithium storage performance has not been the subject of investigation in this study. Heat treatment will transform 1T phase MoS_2 with a larger volume effect into 2H phase MoS_2 with a smaller volume effect, which is beneficial for improving its capacity retention performance. Herein, MoS_2 nanosheets were grown on the surface of the carbon cloth using a hydrothermal reaction and subsequent heat treatment was conducted to increase their electrochemical performance.

2. Experimental Procedure

2.1. Material Synthesis

Carbon cloth (WOS1011, CeTech Co., Ltd., Taiwan, China) was pretreated with 1M nitric acid (Shanghai Titan Scientific Co., Ltd., Shanghai, China) aqueous solution for 3 h, washed several times with deionized water, and then dried at 60 °C for 12 h. Ammonium molybdate tetrahydrate (0.3 g) (Shanghai Titan Scientific Co., Ltd., Shanghai, China) and thiourea (Shanghai Titan Scientific Co., Ltd., Shanghai, China) with the S/Mo molar ratios of 4, 5, and 6 were weighed and then dissolved in 35 mL deionized water under magnetic stirring for 30 min to prepare the solution. The obtained solution and 4 pieces of pretreated carbon cloth (10 mm × 10 mm) were transferred to a Teflon-lined, stainless-steel autoclave (50 mL) and kept at 180 °C for 6 h. After being cooled to room temperature, the carbon cloth with MoS_2 nanosheets was washed several times with deionized water. Subsequently, the washed carbon cloth was dried at 60 °C for 12 h. The MoS_2/carbon cloth composite synthesized with hydrothermal reaction was denoted as MoS_2/CC-No HT. The MoS_2/CC-No HT was placed in the tube furnace under Ar atmosphere, then sintered at 500 °C and maintained for 2 h with a heating rate of 3 °C min^{-1}. The obtained MoS_2/carbon cloth composite was denoted as MoS_2/CC-HT. For comparison, MoS_2 powder was synthesized without the addition of carbon cloth. The MoS_2 powder synthesized with hydrothermal reaction was denoted as MoS_2-No HT. The MoS_2 powder synthesized with hydrothermal reaction and subsequent heat treatment was denoted as MoS_2-HT.

2.2. Material Characterizations

X-ray diffractometer (XRD, Panalytical X'Pert3 Powder, PANalytical B.V., Almelo, The Netherlands) was utilized to measure crystal structure. X-ray photoelectron spectroscopy (XPS, Thermo Scientific K-Alpha, Thermo Fisher Scientific, Waltham, MA, USA) was employed to analyze the chemical state and elemental valence of the samples. Scanning electron microscope (SEM, Hitachi S4800, Hitachi, Tokyo, Japan) and transmission electron microscope (TEM, JEOL JEM-F200, JEOL, Tokyo, Japan) were investigated and used to conduct the morphological observations and microstructural analysis of the samples. An ASAP2460 (Micromeritics, Atlanta, GA, USA) instrument was used to test the specific surface area and pore structure.

2.3. Electrochemical Measurements

The electrochemical performance of the composites was assessed utilizing CR2032-type half coin cells. The coin cells were assembled in a glove box with both H_2O and O_2 contents below 0.1 ppm. MoS_2/CC-HT and MoS_2/CC-No HT were utilized as working electrodes without any intervening steps. The weight of the active substances loaded on the carbon cloth was calculated to be approximately 2.3 ± 0.2 mg cm^{-2}. For MoS_2-HT and MoS_2-No HT powders, it is necessary to fabricate working electrodes before the assembly

of coin cells. The powder samples were prepared as a uniform and stable slurry by mixing the active materials, carbon black, and polyvinylidene fluoride (PVDF) in N-methyl-2-pyrrolidone (NMP) solvent with a weight ratio of 8:1:1. The slurry was applied to the surface of copper foil and dried at 60 °C for 12 h in a vacuum oven. Lithium foil was used as the counter electrode, while the Celgard 2400 membrane functioned as the separator. The electrolyte was 1.0 M $LiPF_6$ in a mixed solution that blended ethylene carbonate (EC), diethyl carbonate (DEC), and methyl ethyl carbonate (EMC) at a volume ratio of 1:1:1. The cyclic voltammetry (CV) and electrochemical impedance spectroscopy (EIS) measurements were performed on the CHI660E (Shanghai Chenhua Instrument Co., Ltd., Shanghai, China) electrochemical workstation. The galvanostatic charge/discharge test was investigated with a Neware-CT3008 instrument (NEWARE Technology Limited, Shenzhen, China).

3. Results and Discussion

Figure 1 shows the SEM images of MoS_2/CC-HT synthesized under different S/Mo molar ratios. The S/Mo molar ratio has a significant effect on the morphology of MoS_2/CC-HT. As exhibited in Figure 1a,b, it can be seen that the MoS_2 in MoS_2/CC-HT synthesized under the S/Mo molar ratio of 5 is ultra-thin nanosheets. In Figure 1c, the MoS_2 in MoS_2/CC-HT synthesized under the S/Mo molar ratio of 6 shows a similar morphology to the MoS_2 in MoS_2/CC-HT synthesized under the S/Mo molar ratio of 5. From Figure 1d, it can be observed that the MoS_2 in MoS_2/CC-HT synthesized under the S/Mo molar ratio of 4 is composed of particles with the size of 50–200 nm and flower-like nanostructure assembled by nanosheets. Ultra-thin nanosheets will provide many electrochemical reaction sites, decrease the diffusion distance of lithium ions, and reduce the absolute volume change caused by lithiation–delithiation due to their large specific surface area and ultra-thin thickness. Therefore, in the following results and discussion, MoS_2/CC-HT and MoS_2/CC-No HT were synthesized under the S/Mo molar ratio of 5. For comparison, MoS_2-HT and MoS_2-No HT were also synthesized under the S/Mo molar ratio of 5. MoS_2/CC-HT and MoS_2/CC-No HT have the same morphology. Heat treatment at 500 °C only changes the phase of MoS_2/CC-No HT (see the XRD analysis in Figure 2), not its morphology.

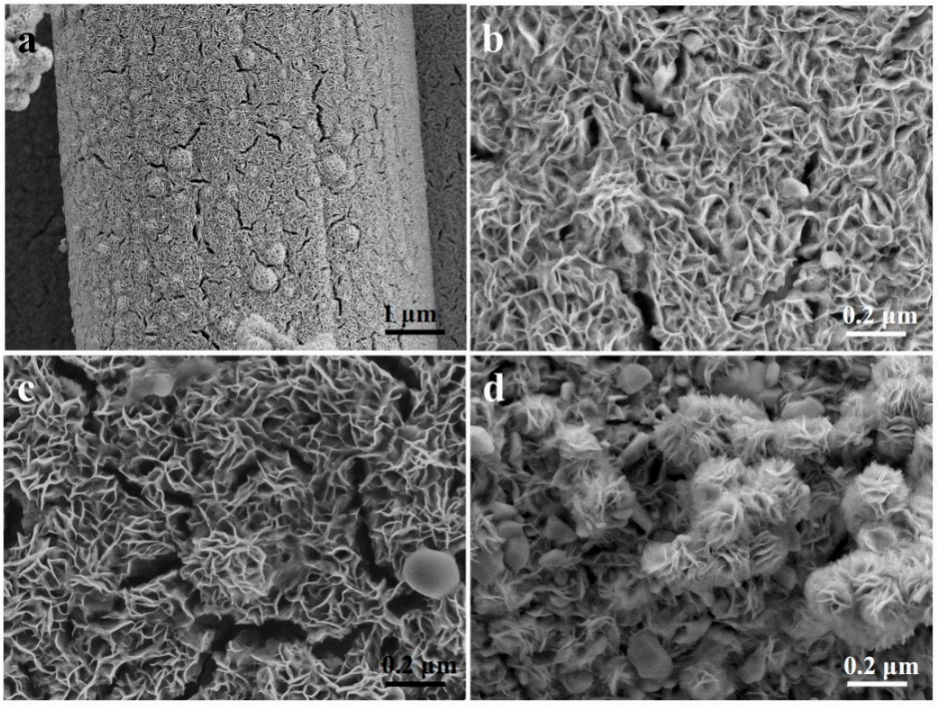

Figure 1. SEM images of MoS_2/CC-HT synthesized under the different S/Mo molar ratios of: (**a**,**b**) 5; (**c**) 6; (**d**) 4.

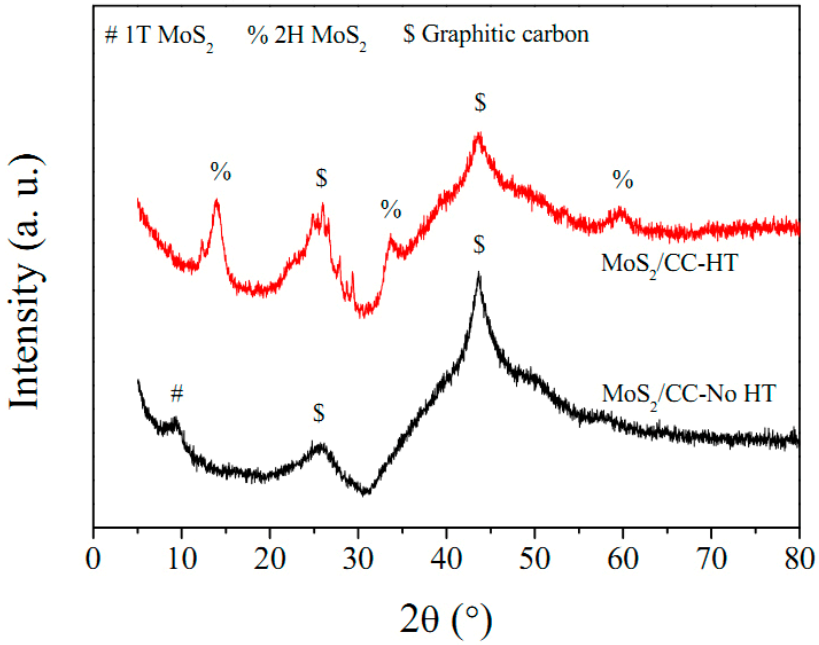

Figure 2. XRD patterns of MoS_2/CC-HT and MoS_2/CC-No HT.

Figure 2 illustrates the XRD patterns for MoS_2/CC-HT and MoS_2/CC-No HT. Two peaks at 25.6 and 43.6° correspond to the (002) and (100) crystal planes of graphitic carbon, respectively. These characteristic XRD peaks are from the carbon cloth [23–25]. In the XRD pattern of MoS_2/CC-No HT, the peak detected at 9.4° is assigned to the (002) crystal plane of 1T phase MoS_2 [26,27]. The peak intensity is weak, indicating the low crystallinity of the MoS_2. In the XRD pattern of MoS_2/CC-HT, the peaks observed at 13.8, 33.6, and 59.5° are attributed to the (002), (100), and (110) crystal planes, respectively, of 2H phase MoS_2 (JCPDS No. 37-1492). The increase in peak intensity indicates an increase in the crystallinity of the 2H phase MoS_2. According to the Scherrer equation, the average grain size of the 2H phase MoS_2 is 9.9 nm. The grain boundaries are rich in defects which provide channels for the diffusion of lithium ions. Thus, the ultrafine average grain size is conducive to the diffusion of lithium ions in the electrode.

X-ray photoelectron spectroscopy (XPS) is used to analyze the chemical states and surface elemental composition of MoS_2/CC-HT. As shown in Figure 3a, the XPS survey spectrum of MoS_2/CC-HT, the spectrum exhibits characteristic peaks of Mo 3d, S 2p, C 1s, and O 1s, indicating the existence of MoS_2 and carbon in MoS_2/CC-HT. The characteristic peaks of O 1s are attributed to the water absorbed on the surface of MoS_2/CC-HT. The center, FWHM, and area percentage for the deconvoluted peaks of Mo 3d, S 2p, and C 1s are presented in Tabs. S1 to S3, respectively (Supplementary Materials). Figure 3b shows the XPS high-resolution spectrum of Mo 3d. The peaks at 232.76 and 229.61 eV are related to Mo $3d_{3/2}$ and Mo $3d_{5/2}$ of Mo^{4+} in MoS_2, respectively [28,29]; the peaks at 234.03 and 230.98 eV assigned to Mo $3d_{3/2}$ and Mo $3d_{5/2}$ of Mo^{6+} are related to the Mo-O-C bond between carbon fibers and MoS_2 nanosheets [23,30]; the peak at 226.78 eV corresponds to S 2s in MoS_2. Figure 3c shows the high-resolution XPS spectrum of S 2p; the separated peaks at 163.59 and 162.40 eV correspond to S $2p_{1/2}$ and S $2p_{3/2}$ of S^{2-}, respectively [31]. In Figure 3d, the XPS high-resolution spectrum of C 1s exhibited two separated peaks at 284.80 and 285.77 eV, which are assigned to C-C and C-O bonds, respectively [28,32].

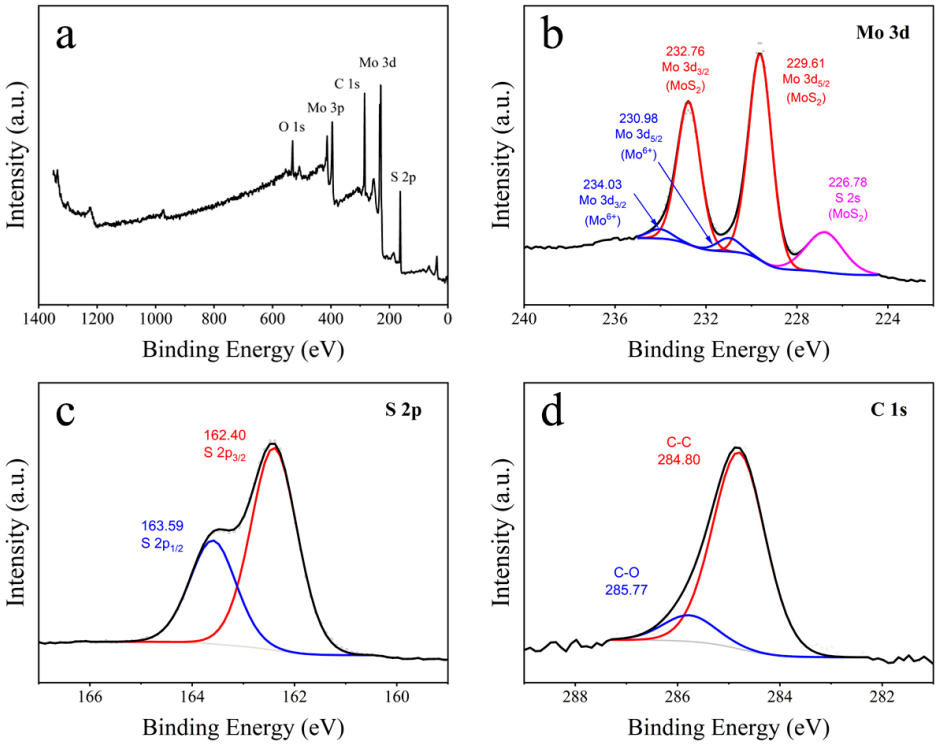

Figure 3. XPS spectra of MoS_2/CC-HT: (**a**) overall spectrum; (**b**) Mo 3d; (**c**) S 2p; (**d**) C 1s.

The TEM, HRTEM, and SAED analyses of MoS_2 in MoS_2/CC-HT are shown in Figure 4. The MoS_2 in MoS_2/CC-HT exhibits a sheet-like structure (Figure 4a), and the lattice fringes of MoS_2 can be observed at its edges (Figure 4b). Figure 4c demonstrates the HRTEM image of MoS_2. It can be seen that its lattice stripes are irregular. The crystal plane spacing of ~0.27 nm corresponds to the (100) crystal plane of 2H phase MoS_2 (JCPDS No. 37-1492). The SAED image of MoS_2 presented in Figure 4d illustrates its polycrystalline characteristics. The diffraction rings can be labeled as the (100) and (110) crystal planes of 2H phase MoS_2 (JCPDS No. 37-1492).

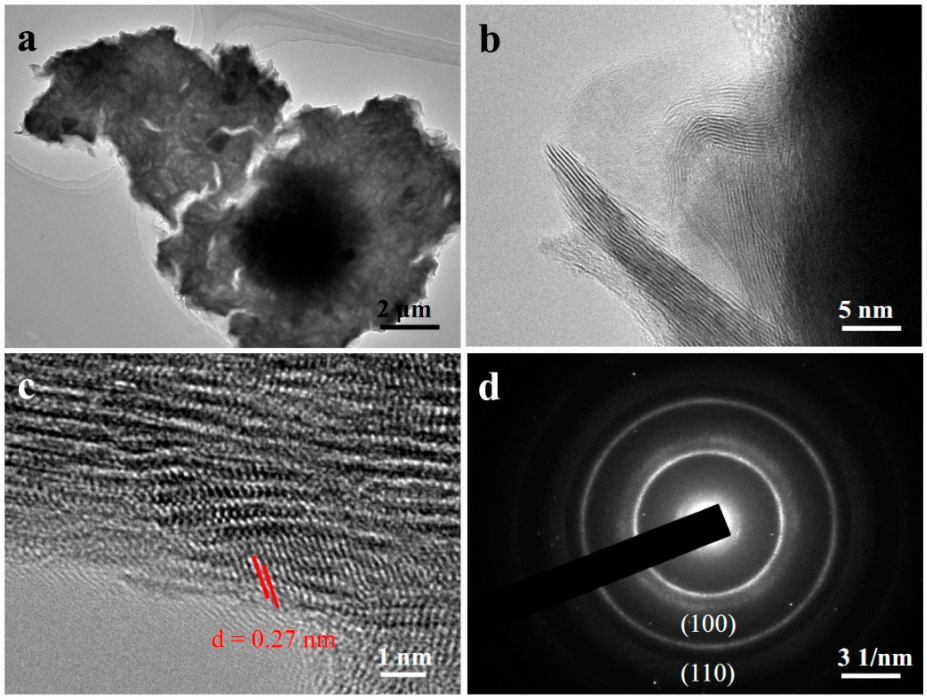

Figure 4. MoS_2/CC-HT: (**a**,**b**) TEM images; (**c**) HRTEM image; (**d**) SAED pattern.

The specific surface area and pore structure analysis of MoS_2/CC-HT and the carbon cloth are demonstrated in Figure 5. From Figure 5a, it can be seen that the N_2 adsorption–desorption isotherms of MoS_2/CC-HT and the carbon cloth belong to Type IV [33]. Calculated with the BET method, the specific surface areas of MoS_2/CC-HT and the carbon cloth are 2.41 and 0.86 $m^2\ g^{-1}$, respectively [33]. By removing the influence of the carbon cloth, it can be estimated that the specific surface area of MoS_2 in MoS_2/CC-HT is ~10.16 $m^2\ g^{-1}$. From Figure 5b, it can be seen that MoS_2/CC-HT has a rich micro-porous structure. The large specific surface area and rich micro-porous structure will increase electrochemical reaction sites and promote the lithium-ion diffusion in the electrode.

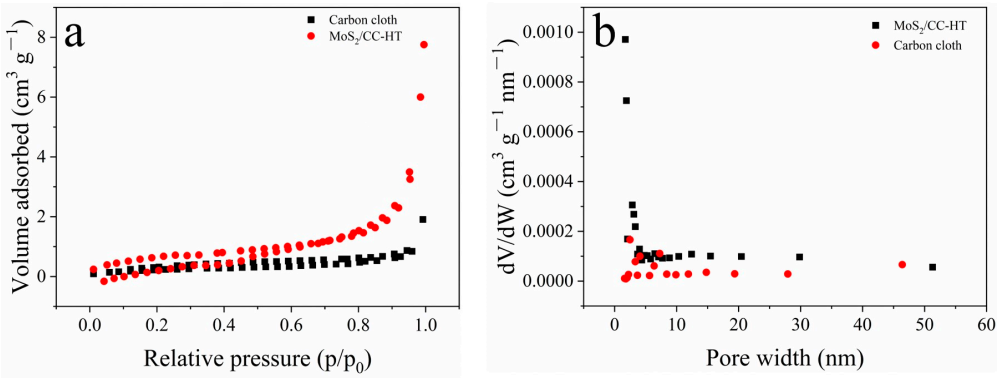

Figure 5. MoS_2/CC-HT and carbon cloth: (**a**) N_2 adsorption-desorption isotherms; (**b**) pore size distribution curves.

MoS_2/CC-HT is composed of MoS_2 and a carbon cloth. Thus, the electrochemical reactions related to its charge–discharge can be described by the following equations [23,28,32]:

$$MoS_2 + xLi^+ + xe^- \rightarrow Li_xMoS_2 \quad (1)$$

$$Li_xMoS_2 + (4 - x)Li^+ + (4 - x)e^- \rightarrow Mo + 2Li_2S \quad (2)$$

$$2Li_2S - 4e^- \rightarrow 2S + 4Li^+ \quad (3)$$

$$Mo + 2Li_2S - 4e^- \rightarrow MoS_2 + 4Li^+ \quad (4)$$

$$Li + C + xe^- \leftrightarrow Li_xC \quad (5)$$

Figure 6a demonstrates the CV curves of the carbon cloth. In the first scanning, the cathode peak around 0.01 V corresponds to Li^+ insertion into the carbon cloth and the formation of solid electrolyte interface (SEI) film, and the anode peak at 0.48 V corresponds to Li^+ de-insertion in the carbon cloth [34]. In the second scanning, the cathode peaks at 0.01, 0.27, and 0.69 V are related to Li^+ insertion of the carbon cloth, and the anode peak at 0.38 V is related to Li^+ de-insertion of the carbon cloth. In the third scanning, the cathode peaks at 0.01, 0.19 and 0.81 V can be assigned to Li^+ insertion of the carbon cloth, and the anode peak at 0.38 V can be assigned to Li^+ de-insertion of the carbon cloth. Figure 6b demonstrates the CV curves of MoS_2/CC-HT. In the first cathode scanning, the two cathode peaks appear at 1.52 and 1.02 V, which are attributed to the insertion of Li^+ into the MoS_2 layer to form Li_xMoS_2 [35]; the cathode peak at 0.53 V is attributed to the formation of an SEI film, accompanied by the decomposition of Li_xMoS_2 to form metal Mo and Li_2S [36], whereas the cathode peak at 0.01 V is attributed to the intercalation of Li^+ in the carbon cloth. In the first anode scanning, the anode peak at 0.26 V is related to the de-intercalation Li^+ in the carbon cloth, while the anode peak at 2.19 V is related to the oxidation process of LiS_2 to S and Mo to MoS_2 [37]. The CV curves of the second and third cycles almost coincide with each other, indicating that MoS_2/CC-HT has good cyclic repeatability. In the second and third scanning, the cathode peak related to the formation

of Li_xMoS_2 by the insertion of Li^+ in MoS_2 layers shifts to 1.93 V; the cathode peak related to the decomposition of Li_xMoS_2 to metallic Mo and Li_2S shifts to 1.12 V [38]; the anode peaks at 0.01, 0.21, and 0.82 V can be assigned to the Li^+ insertion of the carbon cloth.

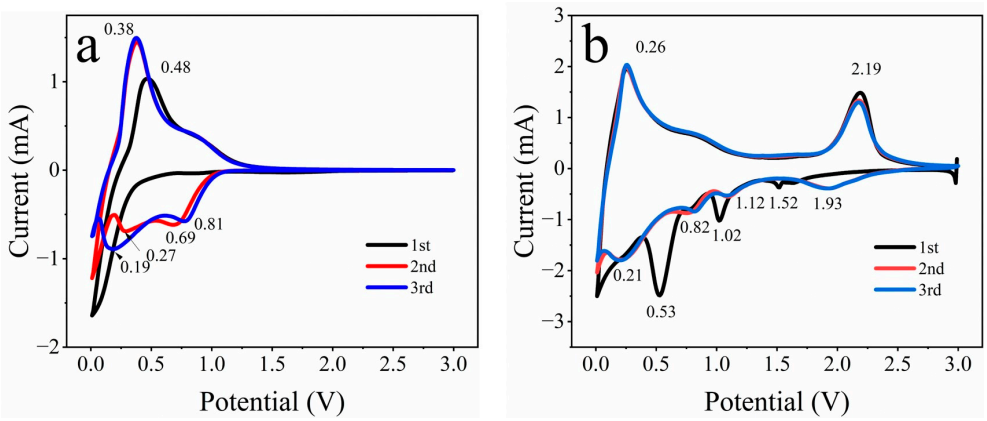

Figure 6. CV curves of: (**a**) carbon cloth; (**b**) MoS_2/CC-HT.

Figure 7a demonstrates the charge–discharge curves of the carbon cloth. The discharge capacities of the carbon cloth are 141, 122, and 114 mAh g^{-1} in the first three cycles; its charge capacities are 129, 120, and 113 mAh g^{-1}; and its Coulombic efficiencies are 91.5%, 98.4%, and 99.1%. In Figure 7b, the charge–discharge profiles of MoS_2/CC-HT and the charge voltage plateau at 2.19 V corresponds to the oxidation of LiS_2 to S and Mo to MoS_2. The discharge capacities of MoS_2/CC-HT are 1478, 1296, and 1245 mAh g^{-1} in the first three cycles; its charge capacities are 1370, 1274, and 1234 mAh g^{-1}; and its Coulombic efficiencies are 92.7%, 98.3%, and 99.1%.

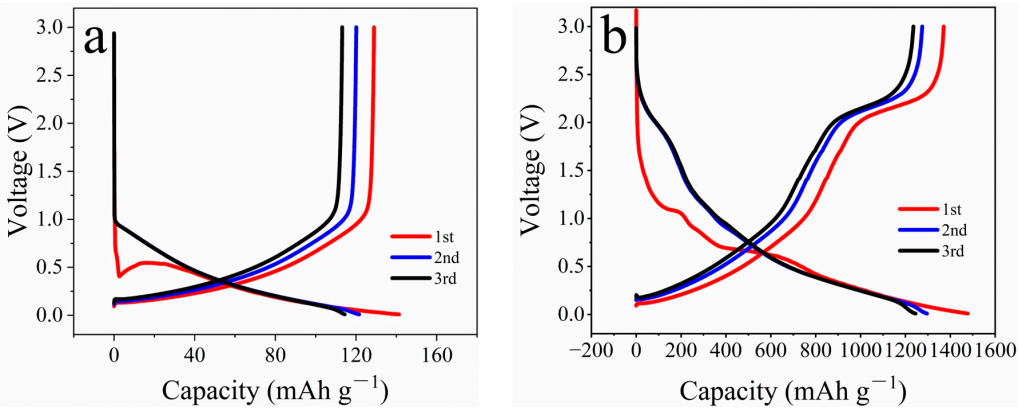

Figure 7. Charge–discharge profiles of: (**a**) carbon cloth; (**b**) MoS_2/CC-HT.

The cyclic performance of MoS_2/CC-HT, MoS_2/CC-No HT, and the carbon cloth are shown in Figure 8a. The carbon cloth delivers a stable capacity of 110 mAh g^{-1} during cycling. The capacities of MoS_2/CC-HT and MoS_2/CC-No HT include the capacity of the carbon cloth and the capacity of MoS_2 loaded on the surface of the carbon cloth. Therefore, the capacity of MoS_2 in MoS_2/CC-No HT and MoS_2 in MoS_2/CC-No HT (shown in Figure 8b) can be calculated by removing the capacity of the carbon cloth. The capacity of MoS_2 in MoS_2/CC-HT continuously increases to 1075 mAh g^{-1} at a current density of 0.1 A g^{-1} after 50 cycles, while the capacity of MoS_2 in MoS_2/CC-No HT continuously decreases to 528 mAh g^{-1}. The MoS_2 in MoS_2/CC No HT is 1T phase, while the MoS_2 in MoS_2/CC HT is the 2H phase; 2H phase MoS_2 has a better capacity retention performance than 1T phase MoS_2. Therefore, with heat treatment, MoS_2 on the surface of the carbon cloth is transformed from the 1T phase to the 2H phase, resulting in the better capacity retention performance of MoS_2/CC-HT.

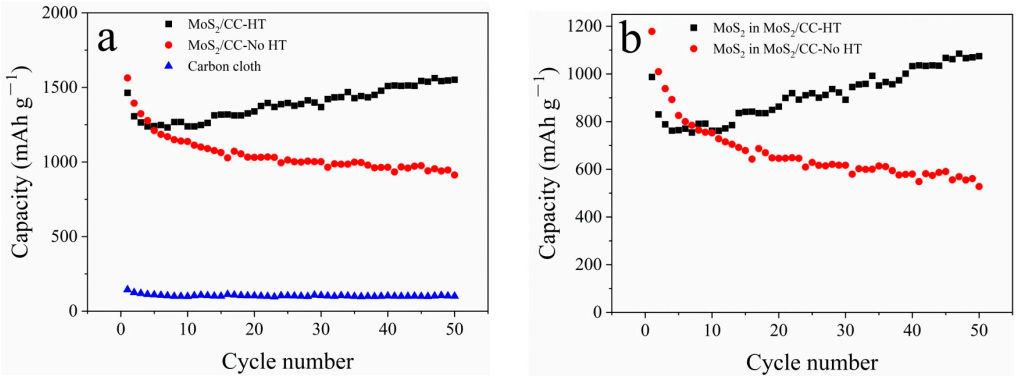

Figure 8. Cyclic performance: (**a**) MoS_2/CC-HT, MoS_2/CC-No HT, and carbon cloth; (**b**) MoS_2 in MoS_2/CC-HT and MoS_2 in MoS_2/CC-No HT.

The rate performance of MoS_2/CC-HT, MoS_2/CC-No HT, and the carbon cloth are demonstrated in Figure 9a. By removing the capacity of the carbon cloth, the rate performance of MoS_2 in MoS_2/CC-HT and MoS_2 in MoS_2/CC-No HT is presented in Figure 9b. MoS_2 in MoS_2/CC-HT delivers the capacities of 775, 802, 826, 790, and 663 mAh g^{-1} at current densities of 0.1, 0.2, 0.5, 1, and 2 A g^{-1}, demonstrating its good rate performance. When the current density returns to 0.1 A g^{-1}, it delivers a capacity of 991 mAh g^{-1}, which is higher than its initial capacity at the current density of 0.1 A g^{-1}. MoS_2 in MoS_2/CC-No HT delivers the capacities of 902, 652, 550, 453, and 311 mAh g^{-1} at the current densities of 0.1, 0.2, 0.5, 1, and 2 A g^{-1}. When the current density returns to 0.1 A g^{-1}, it delivers the capacity of 654 mAh g^{-1}, which is lower than its initial capacity at the current density of 0.1 A g^{-1}. The larger volume change of 1T phase MoS_2 during charge–discharge leads to the worse capacity retention performance of MoS_2/CC-No HT.

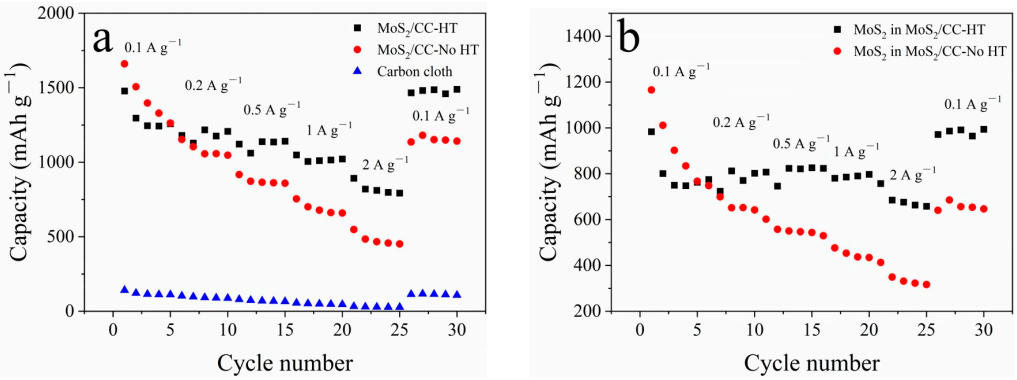

Figure 9. Rate performance: (**a**) MoS_2/CC-HT, MoS_2/CC-No HT, and carbon cloth; (**b**) MoS_2 in MoS_2/CC-HT and MoS_2 in MoS_2/CC-No HT.

Figure 10 demonstrates the cyclic and rate performance of MoS_2-HT and MoS_2-No HT powders. From Figure 10a, it can be seen that MoS_2-HT powder has a better capacity retention performance than MoS_2-No HT powder. MoS_2-HT delivers a capacity of 401 mAh g^{-1}, while MoS_2-No HT delivers a capacity of 258 mAh g^{-1} at a current density of 0.1 A g^{-1} after 50 cycles. During charge–discharge, 1T phase MoS_2-No HT undergoes a larger volume change than 2H phase MoS_2-HT, which leads to its worse capacity retention performance. From Figure 10b, at the gradually increasing current densities of 0.1, 0.2, 0.5, 1, and 2 A g^{-1}, MoS_2-HT delivers the capacities of 709, 616, 601, 427, and 363 mAh g^{-1}, while MoS_2-No HT delivers the capacities of 746, 578, 128, 57, and 27 mAh g^{-1}.

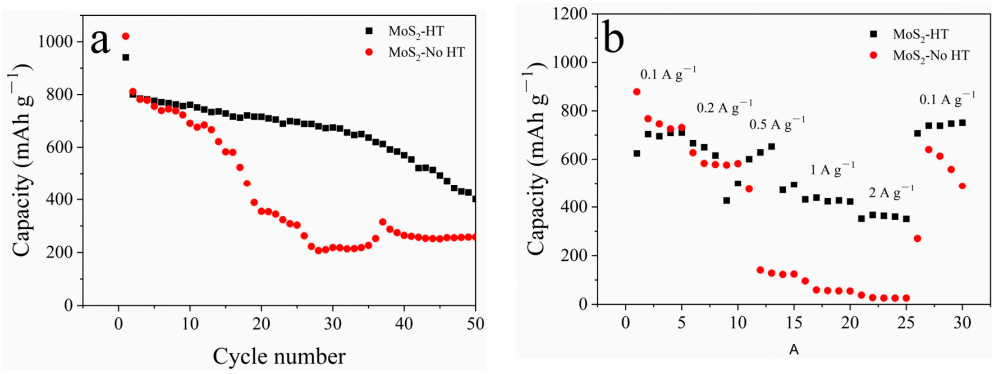

Figure 10. MoS_2-HT and MoS_2-No HT powder: (**a**) cyclic performance; (**b**) rate performance.

Figure 11a shows the XRD patterns of MoS_2-HT and MoS_2-No HT powders. It can be seen that MoS_2-HT is 2H phase, while MoS_2-No HT is 1T phase, indicating that the carbon cloth substrate will not change the phase of the loaded MoS_2. Figure 11b,c demonstrate the SEM image of MoS_2-No HT and MoS_2-HT powder, respectively. Because heat treatment only changes the phase of MoS_2, MoS_2-No HT powder exhibits the same morphology as MoS_2-HT powder. From Figure 11b,c, it can be seen that both MoS_2-No HT powder and MoS_2-HT powder consist of MoS_2 flowers (area outside the red ring in Figure 11b,c) and MoS_2 aggregates (area inside the red ring in Figure 11b,c). Because MoS_2 in this paper is synthesized by a hydrothermal reaction in an aqueous solution of ammonium molybdate and thiourea, the strong polarity of water inevitably leads to the aggregation of the synthesized MoS_2. Large-sized MoS_2 aggregates will undergo fragmentation, pulverization, and detachment during the charge–discharge, resulting in their capacity fading. The carbon cloth substrate causes the loaded MoS_2 to form a mutually separated nanosheet array. The non-agglomerated MoS_2 nanosheet array will increase electrochemical reaction sites and promote the diffusion of lithium ions in the electrode. Thus, MoS_2/CC-HT delivers higher capacity than MoS_2-HT, while MoS_2/CC-No HT delivers higher capacity than MoS_2-No HT.

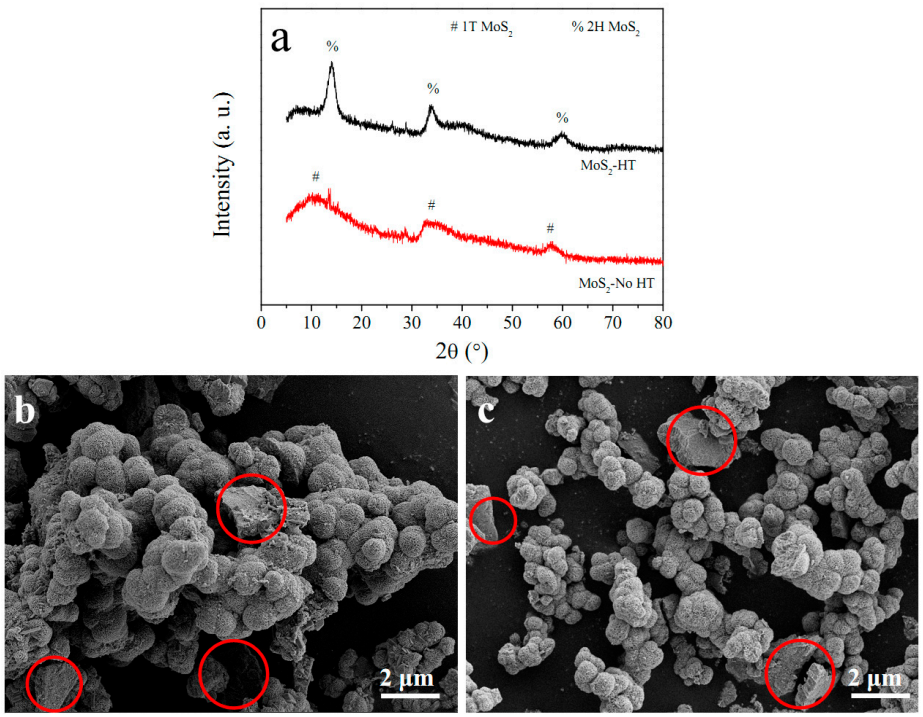

Figure 11. (**a**) XRD patterns of MoS_2-HT and MoS_2-No HT; SEM images of (**b**) MoS_2-No HT and (**c**) MoS_2-HT.

Figure 12 presents the EIS patterns of MoS_2/CC-HT, MoS_2/CC-No HT, MoS_2-HT, and MoS_2-No HT. In the mid-frequency region, the diameter of the semicircle in the Nyquist plot is related to the charge transfer resistance of the electrode [39,40]. The larger semicircle diameter means the larger charge transfer resistance of the electrode. The charge transfer resistances of MoS_2/CC-HT, MoS_2/CC-No HT, MoS_2-HT, and MoS_2-No HT are 60.2, 245.6, 466.8, and 575.5 Ω, respectively. The carbon cloth has good conductivity. The conductivity of the loaded MoS_2 nanosheets can be enhanced by the carbon cloth substrate, thereby reducing their charge transfer resistance. In the low-frequency region, the slope of the oblique line in the Nyquist plot is related to the diffusion rate of lithium ions in the electrode. The steeper the slope of the oblique line, the faster the rate of diffusion of lithium ions into the electrode [41]. Apparently, the diffusion rate of lithium ions in MoS_2/CC-HT is faster than that in MoS_2-HT, and the diffusion rate of lithium ions in MoS_2/CC-No HT is faster than that in MoS_2-No HT. The mutually separated MoS_2 nanosheets grown on the surface of the carbon cloth will promote the diffusion of lithium ions in the electrode.

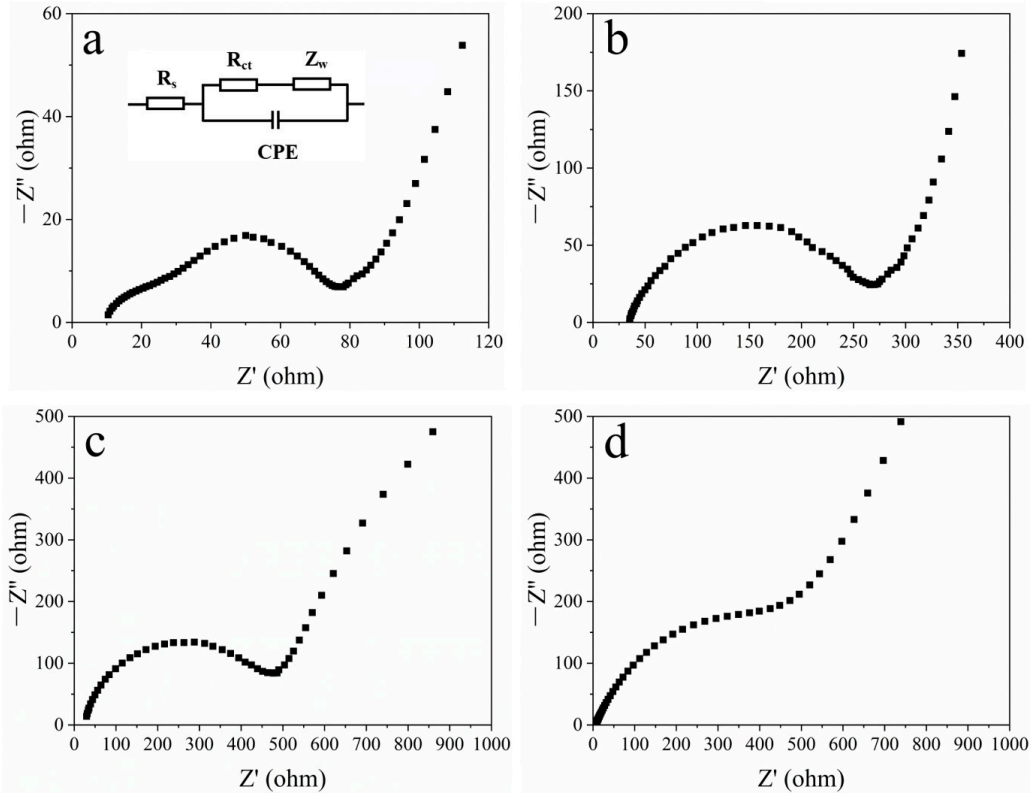

Figure 12. EIS patterns of: (**a**) MoS_2/CC-HT (equivalent circuit in inset); (**b**) MoS_2/CC-No HT; (**c**) MoS_2-HT; (**d**) MoS_2-No HT.

Figure 13a,b provide the SEM images of MoS_2/CC-HT after 50 cycles at a current density of 0.1 A g^{-1}. The MoS_2 layer still firmly adhered to the surface of the carbon cloth without shedding. In contrast, for MoS_2/CC-No HT after cycling, a large amount of detachment occurred in the MoS_2 layer (Figure 13c,d). This is the reason why MoS_2/CC-HT has a better capacity retention performance than MoS_2/CC-No HT.

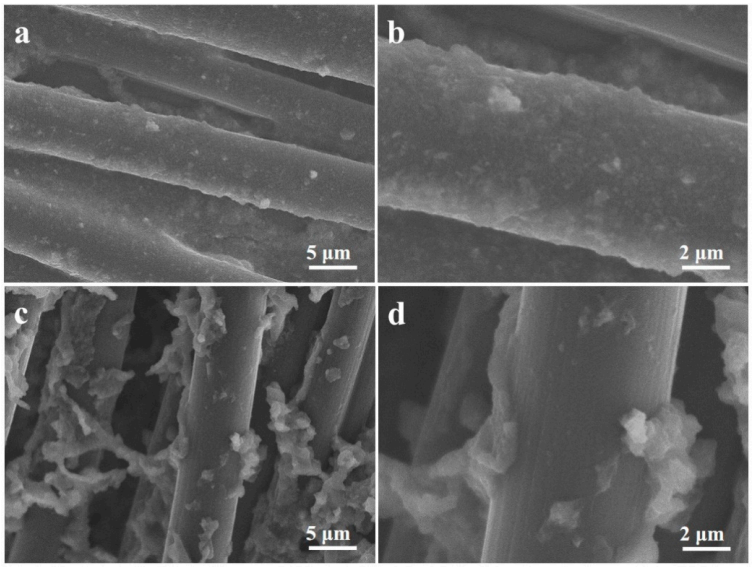

Figure 13. SEM images of: (**a**,**b**) MoS_2/CC-HT after cycling; (**c**,**d**) MoS_2/CC-No HT after cycling.

4. Conclusions

In this paper, ammonium molybdate and thiourea were employed as raw materials to synthesize a MoS_2/carbon cloth composite via a hydrothermal reaction. Under the S/Mo molar ratio of 5, the grown MoS_2 on the surface of the carbon cloth is ultra-thin nanosheets. MoS_2 in MoS_2/CC-No HT synthesized using a hydrothermal reaction is the 1T phase. After heat treatment, it transforms into the 2H phase while maintaining its morphology.

As an anode material for LIBs, the MoS_2 in MoS_2/CC-HT delivers a continuously increasing capacity of 1075 mAh g^{-1} at a current density of 0.1 A g^{-1} after 50 cycles, while the MoS_2 in MoS_2/CC-No HT delivers a fading capacity of 528 mAh g^{-1}. With heat treatment, MoS_2 on the surface of the carbon cloth is transformed from the 1T phase to the 2H phase with a better capacity retention performance, resulting in the better capacity retention performance of MoS_2/CC-HT.

MoS_2 powder synthesized without the carbon cloth substrate consists of MoS_2 flowers and MoS_2 aggregates. Aggregates reduce the electrochemical reaction sites and hinder the diffusion of lithium ions in the electrode, which decrease their electrochemical performance. The carbon cloth substrate can improve the conductivity of loaded MoS_2 nanosheets and prevent them from agglomerating, which increases their capacity, reduces their charge transfer resistance, and promotes the diffusion of lithium ions in the electrode.

A carbon cloth with good conductivity and mechanical flexibility is an appropriate current collector for a flexible LIBs electrode. In this paper, a simple heat treatment route was employed to synthesize a MoS_2/carbon cloth composite with a high capacity and good capacity retention performance. This composite is expected to be applied in wearable electronic devices.

Supplementary Materials: The following supporting information can be downloaded at: https://www.mdpi.com/article/10.3390/ma16247678/s1, Table S1: Centre, FWHM and percentage area (area%) for the deconvoluted peaks of Mo 3d. Table S2: Centre, FWHM and percentage area (area%) for the deconvoluted peaks of S 2p. Table S3: Centre, FWHM and percentage area (area%) for the deconvoluted peaks of C 1s.

Author Contributions: Conceptualization, X.L.; methodology, C.L.; validation, X.L. and Q.Y.; formal analysis, X.L.; investigation, X.L.; resources, Q.Y. and C.L.; data curation, X.L.; writing—original draft preparation, X.L.; writing—review and editing, X.L. and Q.Y.; visualization, X.L.; supervision, Q.Y.; project administration, C.L.; funding acquisition, C.L. All authors have read and agreed to the published version of the manuscript.

Funding: This work was funded by the Open Fund of the Key Laboratory of Equipment Pre-Research and Class III Peak Discipline of Shanghai-Materials Science and Engineering (High-Energy Beam Intelligent Processing and Green Manufacturing).

Data Availability Statement: Data are contained within the article.

Conflicts of Interest: The authors declare no conflict of interest.

References

1. Zubi, G.; Dufo-López, R.; Carvalho, M.; Pasaoglu, G. The lithium-ion battery: State of the art and future perspectives. *Renew. Sustain. Energy Rev.* **2018**, *89*, 292–308. [CrossRef]
2. Tarascon, J.M.; Armand, M. Issues and challenges facing rechargeable lithium batteries. *Nature* **2001**, *414*, 359–367. [CrossRef] [PubMed]
3. Vishnumurthy, K.A.; Girish, K.H. A comprehensive review of battery technology for E-mobility. *J. Indian Chem. Soc.* **2021**, *98*, 100173. [CrossRef]
4. Camargos, P.H.; dos Santos, P.H.J.; dos Santos, I.R.; Ribeiro, G.S.; Caetano, R.E. Perspectives on Li-ion battery categories for electric vehicle applications: A review of state of the art. *Int. J. Energy Res.* **2022**, *46*, 19258–19268. [CrossRef]
5. Kim, T.; Song, W.; Son, D.-Y.; Ono, L.K.; Qi, Y. Lithium-ion batteries: Outlook on present, future, and hybridized technologies. *J. Mater. Chem. A* **2019**, *7*, 2942–2964. [CrossRef]
6. Asenbauer, J.; Eisenmann, T.; Kuenzel, M.; Kazzazi, A.; Chen, Z.; Bresser, D. The success story of graphite as a lithium-ion anode material—Fundamentals, remaining challenges, and recent developments including silicon (oxide) composites. *Sustain. Energy Fuels* **2020**, *4*, 5387–5416. [CrossRef]
7. Ali, H.G.; Khan, K.; Hanif, M.B.; Khan, M.Z.; Hussain, I.; Javed, M.S.; AL-bonsrulah, H.A.Z.; Mosiałek, M.; Fichtner, M.; Motola, M. Advancements in two-dimensional materials as anodes for lithium-ion batteries: Exploring composition-structure-property relationships emerging trends, and future perspective. *J. Energy Storage* **2023**, *73*, 108980. [CrossRef]
8. Shajaripour Jaberi, S.Y.; Ghaffarinejad, A.; Khajehsaeidi, Z.; Sadeghi, A. The synthesis, properties, and potential applications of CoS_2 as a transition metal dichalcogenide (TMD). *Int. J. Hydrogen Energy* **2023**, *48*, 15831–15878. [CrossRef]
9. Mensah-Darkwa, K.; Nframah Ampong, D.; Agyekum, E.; de Souza, F.M.; Gupta, R.K. Recent Advancements in Chalcogenides for Electrochemical Energy Storage Applications. *Energies* **2022**, *15*, 4052. [CrossRef]
10. Theerthagiri, J.; Senthil, R.A.; Senthilkumar, B.; Polu, A.R.; Madhavan, J.; Ashokkumar, M. Recent advances in MoS_2 nanostructured materials for energy and environmental applications—A review. *J. Solid State Chem.* **2017**, *252*, 43–71. [CrossRef]
11. Baheri, Y.T.; Hedayati, M.A.; Maleki, M.; Karimian, H. A vapor-liquid-solid mechanism for in-situ deposition of ultra-small hollow MoS_2 nanoparticles in N-doped carbon foam as an anode of lithium-ion batteries. *J. Energy Storage* **2023**, *68*, 107682. [CrossRef]
12. Barik, G.; Pal, S. 2D Square Octagonal Molybdenum Disulfide: An Effective Anode Material for LIB/SIB Applications. *Adv. Theory Simul.* **2020**, *3*, 2000157. [CrossRef]
13. Yang, F.; Feng, X.; Glans, P.-A.; Guo, J. MoS_2 for beyond lithium-ion batteries. *APL Mater.* **2021**, *9*, 050903. [CrossRef]
14. Yun, Q.; Li, L.; Hu, Z.; Lu, Q.; Chen, B.; Zhang, H. Layered Transition Metal Dichalcogenide-Based Nanomaterials for Electrochemical Energy Storage. *Adv. Mater.* **2020**, *32*, 1903826. [CrossRef] [PubMed]
15. Li, X.L.; Li, T.C.; Huang, S.; Zhang, J.; Pam, M.E.; Yang, H.Y. Controllable synthesis of 2D Molybdenum Disulfide (MoS_2) for energy storage applications. *ChemSusChem* **2020**, *13*, 1379–1391. [CrossRef] [PubMed]
16. Febrian, R.; Septiani, N.L.W.; Iqbal, M.; Yuliarto, B. Review—Recent Advances of Carbon-Based Nanocomposites as the Anode Materials for Lithium-Ion Batteries: Synthesis and Performance. *J. Electrochem. Soc.* **2021**, *168*, 110520. [CrossRef]
17. Muchuweni, E.; Mombeshora, E.T.; Muiva, C.M.; Sathiaraj, T.S. Lithium-ion batteries: Recent progress in improving the cycling and rate performances of transition metal oxide anodes by incorporating graphene-based materials. *J. Energy Storage* **2023**, *73*, 109013. [CrossRef]
18. León, M.I.; Castañeda, L.F.; Márquez, A.A.; Walsh, F.C.; Nava, J.L. Review—Carbon Cloth as a Versatile Electrode: Manufacture, Properties, Reaction Environment, and Applications. *J. Electrochem. Soc.* **2022**, *169*, 053503. [CrossRef]
19. Wenelska, K.; Adam, V.; Thauer, E.; Singer, L.; Klingeler, R.; Chen, X.; Mijowska, E. Fabrication of 3D graphene/MoS_2 spherical heterostructure as anode material in Li-ion battery. *Front. Energy Res.* **2022**, *10*, 960786. [CrossRef]
20. Qin, S.; Lei, W.; Liu, D.; Chen, Y. Advanced N-doped Mesoporous Molybdenum Disulfide Nanosheets and the Enhanced Lithium-ion Storage Performance. *J. Mater. Chem. A* **2015**, *4*, 1440–1445. [CrossRef]
21. Patil, S.B.; Kishore, B.; Vishwanatha, R.; Ebeling, G.; Nagaraju, G. CdS@MoS_2 core–shell nanospheres: A new electrode for lithium ion batteries. *J. Mater. Sci. Mater. Electron.* **2019**, *30*, 14456–14463. [CrossRef]
22. Francis, M.K.; Rajesh, K.; Bhargav, P.B.; Ahmed, N. Binder-free phosphorus-doped MoS_2 flexible anode deposited on carbon cloth for high-capacity Li-ion battery applications. *J. Mater. Sci.* **2023**, *58*, 4054–4069. [CrossRef]
23. Wu, M.; Zhan, J.; Wu, K.; Li, Z.; Wang, L.; Geng, B.; Wang, L.; Pan, D. Metallic 1T MoS_2 nanosheet arrays vertically grown on activated carbon fiber cloth for enhanced Li-ion storage performance. *J. Mater. Chem. A* **2017**, *5*, 14061–14069. [CrossRef]
24. Deng, Z.; Jiang, H.; Hu, Y.; Liu, Y.; Zhang, L.; Liu, H.; Li, C. 3D Ordered Macroporous MoS_2@C Nanostructure for Flexible Li-Ion Batteries. *Adv. Mater.* **2017**, *29*, 1603020. [CrossRef] [PubMed]

25. Wang, C.; Wang, X.; Lin, C.; Zhao, X.S. Spherical vanadium phosphate particles grown on carbon fiber cloth as flexible anode for high-rate Li-ion batteries. *Chem. Eng. J.* **2020**, *386*, 123981. [CrossRef]
26. Yang, E.; Wei, N.; Li, M.; Xu, R.; Sui, Y.; Kong, M.; Ran, X.; Cui, H. Three-Dimensional Artificial Transpiration Structure Based on 1T/2H-MoS_2/Activated Carbon Fiber Cloth for Solar Steam Generation. *ACS Appl. Mater. Interfaces* **2022**, *14*, 29788–29796. [CrossRef]
27. Bai, J.; Zhao, B.; Zhou, J.; Si, J.; Fang, Z.; Li, K.; Ma, H.; Dai, J.; Zhu, X.; Sun, Y. Glucose-Induced Synthesis of 1T-MoS_2/C Hybrid for High-Rate Lithium-Ion Batteries. *Small* **2019**, *15*, 1805420. [CrossRef]
28. Lee, D.-Y.; Seo, S.D.; Song, H.J.; Kim, D.-W. Free-standing molybdenum disulfides on porous carbon cloth for lithium-ion battery anodes. *Int. J. Energy Res.* **2021**, *45*, 11329–11337. [CrossRef]
29. Xiao, Z.; Chen, W.; Chen, Z.; Chen, C.; Cao, W.; Yu, F. Stable Sandwich-Like Biomass Carbon@MoS_2 Composite Material with Enhanced Sodium Storage Performance. *Energy Fuels* **2022**, *36*, 3954–3963. [CrossRef]
30. Teng, Y.; Zhao, H.; Zhang, Z.; Li, Z.; Xia, Q.; Zhang, Y.; Zhao, L.; Du, X.; Du, Z.; Lv, P.; et al. MoS_2 Nanosheets Vertically Grown on Graphene Sheets for Lithium-Ion Battery Anodes. *ACS Nano* **2016**, *10*, 8526–8535. [CrossRef]
31. Wang, H.W.; Skeldon, P.; Thompson, G.E. XPS studies of MoS_2 formation from ammonium tetrathiomolybdate solutions. *Surf. Coat. Technol.* **1997**, *91*, 200–207. [CrossRef]
32. Bai, J.; Zhao, B.; Wang, X.; Ma, H.; Li, K.; Fang, Z.; Li, H.; Dai, J.; Zhu, X.; Sun, Y. Yarn ball-like MoS_2 nanospheres coated by nitrogen-doped carbon for enhanced lithium and sodium storage performance. *J. Power Sources* **2020**, *465*, 228282. [CrossRef]
33. Bardestani, R.; Patience, G.S.; Kaliaguine, S. Experimental methods in chemical engineering: Specific surface area and pore size distribution measurements-BET, BJH, and DFT. *Can. J. Chem. Eng.* **2019**, *97*, 2781–2791. [CrossRef]
34. Narsimulu, D.; Nagaraju, G.; Sekhar, S.C.; Ramulu, B.; Yu, J.S. Designed lamination of binder-free flexible iron oxide/carbon cloth as high capacity and stable anode material for lithium-ion batteries. *Appl. Surf. Sci.* **2019**, *497*, 143795. [CrossRef]
35. Xiao, J.; Wang, X.; Yang, X.-Q.; Xun, S.; Liu, G.; Koech, P.K.; Liu, J.; Lemmon, J.P. Electrochemically Induced High Capacity Displacement Reaction of PEO/MoS_2/Graphene Nanocomposites with Lithium. *Adv. Funct. Mater.* **2011**, *21*, 2840–2846. [CrossRef]
36. Jiang, J.; Zhang, Y.; An, Y.; Wu, L.; Zhu, Q.; Dou, H.; Zhang, X. Engineering Ultrathin MoS_2 Nanosheets Anchored on N-Doped Carbon Microspheres with Pseudocapacitive Properties for High-Performance Lithium-Ion Capacitors. *Small Methods* **2019**, *3*, 1900081. [CrossRef]
37. Han, Y.; Chatti, M.; Ge, Y.; Wang, C.; Chao, Y.; Simonov, A.N.; Wallace, G.G. Binder-Free electrodes derived from interlayer-expanded MoS_2 nanosheets on carbon cloth with 3D porous structure for high lithium storage. *ChemElectroChem* **2019**, *6*, 2338–2343. [CrossRef]
38. Xu, Y.; Yan, W.; Sun, X.; Tang, G.; Chen, Y.; Xu, J. Synthesis of 1D-MoS_2/graphene nanotubes aided with sodium chloride for reversible lithium storage. *Ceram. Int.* **2022**, *48*, 7687–7694. [CrossRef]
39. Zhai, N.S.; Li, M.W.; Wang, W.L.; Zhang, D.L.; Xu, D.G. The Application of the EIS in Li-ion Batteries Measurement. *J. Phys. Conf. Ser.* **2006**, *48*, 1157–1161. [CrossRef]
40. Zhuang, Q.; Yang, Z.; Zhang, L.; Cui, Y. Research Progress on Diagnosis of Electrochemical Impedance Spectroscopy in Lithium Ion Batteries. *Prog. Chem.* **2020**, *32*, 761–791.
41. Stolyarova, S.G.; Kotsun, A.A.; Shubin, Y.V.; Koroteev, V.O.; Plyusnin, P.E.; Mikhlin, Y.L.; Mel'gunov, M.S.; Okotrub, A.V.; Bulusheva, L.G. Synthesis of Porous Nanostructured MoS_2 Materials in Thermal Shock Conditions and Their Performance in Lithium-Ion Batteries. *ACS Appl. Energy Mater.* **2020**, *3*, 10802–10813. [CrossRef]